Spectroscopic evidence of quasi-one-dimensional metallic Rashba spin-split states on the Si(111)5 × 2-Au surface

Kazuaki Taguchi,[1] Kazuki Sumida,[1] Yuki Okuda,[1] Koji Miyamoto,[2] Akio Kimura,[1] Tamio Oguchi,[3] and Taichi Okuda[2,*]

[1]*Graduate School of Science, Hiroshima University, 1-3-1 Kagamiyama, Higashi-Hiroshima 739-8526, Japan*

[2]*Hiroshima Synchrotron Radiation Center (HSRC), Hiroshima University, 2-313 Kagamiyama, Higashi-Hiroshima 739-0046, Japan*

[3]*Institute of Scientific and Industrial Research, Osaka University, Osaka 567-0047, Japan*

(Received 17 October 2018; revised manuscript received 8 January 2020; published 29 January 2020)

Spin polarization by Rashba effect in the quasi-one-dimensional metallic bands of Si(111)5 × 2-Au surface is revealed by spin- and angle-resolved photoelectron spectroscopy and the first-principles calculation. Small but clear spin polarization and its sign reversal with respect to the $\overline{\Gamma}$ point is observed indicating the Rashba origin of the spin-polarized states. Deviating from the typical helical tangential spin texture of normal Rashba effect of two-dimensional electronic states, not only in-plane but significant out-of-plane spin polarization probably caused by the anisotropic in-plane charge distribution around Au atoms is observed at some specific k points. The observed peculiar spin texture of the sample is qualitatively in good agreement with the results of the first-principles calculation based on the recently proposed surface reconstruction model by Kwon and Kang implying the validity of the structural model.

DOI: 10.1103/PhysRevB.101.045430

I. INTRODUCTION

Si(111)5 × 2-Au surface is one of the most extensively investigated reconstructed Si surfaces. Well-ordered one-dimensional atomic chain of Au has attracted attention since the system is considered as an ideal playground for the investigation of the exotic one-dimensional phenomena [1–3] such as Peierls instability, Tomonaga-Luttinger liquid, etc. Despite the plenty of experimental and theoretical studies on the surface, however, even the atomic structure of the reconstructed surface has been in a long debate.

The uncertainty of the estimation of Au coverage made the structural investigation very laborious. In accordance with the long-believed Au coverage of $\theta = 0.4$ ML, many models have been proposed [4–7] and these models are experimentally [4–6,8–11] and theoretically examined [7,12–15]. However, none of the proposed models could explain completely all the experimental results such as streaks in low-energy electron diffraction (LEED) pattern [4], Y-shaped structure and protrusions in the scanning tunneling microscope (STM) image [10], and complicated surface band dispersion by angle-resolved photoelectron spectroscopy (ARPES) [11]. However, Barke and coworkers reinvestigated the Au coverage by comparing with the well-established Si(557)-Au surface [16] and Erwin, Barke, and Himpsel (EBH) proposed the new model compatible with the observed Au coverage of 0.57–0.65 ML [17]. The first-principles calculation based on this so-called EBH model could reproduce many of the experimental results such as STM image and electronic band structure observed by ARPES. One big drawback of the EBH model is, however, the lack of the intrinsic 5 × 2 periodicities and the aid of Si adatoms or electron doping is needed to explain the observed 5 × 2 periodicity. Later on, Abukawa and Nishigawa proposed the alternative model with 0.6 ML (AN model), which has intrinsic 5 × 2 periodicities, by the detailed analysis of a reflection high-energy electron diffraction (RHEED) data [18]. However, the structure could not pass the examination by the recent density functional theory (DFT) calculation which indicates that the structure is not energetically favorable compared with the EBH model [19]. Although it was denied, the AN model reheated the exploration of the real structural model of the 5 × 2-Au surface. After a short while, Kwon and Kang demonstrated that the most stable 5 × 2 reconstruction can be obtained by adding one more Au atom into the EBH model [20]. Although this modification results in the Au coverage of 0.7 ML, it is still in the acceptable range of the estimated amount of Au. The Kwon and Kang's model (KK model) can also reproduce the STM images and the ARPES results as well as some other properties reported by the previous experiments. In addition, the recent x-ray diffraction measurement also supports the model [21]. Thus, the KK model is the most plausible structural model of Si(111)5 × 2-Au surface among the models proposed so far.

As already mentioned, the electronic structure of the surface has also been investigated extensively. ARPES observation shows the complicated band structures [22–24]. Although the bands are in principle possessing one-dimensional character the transition to the two-dimensional character at higher binding energies has been also reported [11]. Some of the surface bands are crossing Fermi level indicating metallic character but the reduction of photoemission intensity near the Fermi level is also observed.

Although it has not been addressed so far, the other interesting issue of the electronic structure of the sample is a possible spin splitting by the Rashba effect which can be

*okudat@hiroshima-u.ac.jp

caused by the strong spin-orbit interaction (SOI) of Au. Actually, in the Au-deposited vicinal Si(111) surfaces like Si(553)-Au and Si(557)-Au, which have many similarities with the Si(111)5 × 2-Au, a clear splitting of the surface state band has been observed [22,25,26] and the experimental and theoretical evidences of spin-split states caused by SOI have been reported [27–30]. In addition, unlike the conventional Rashba effect in the two-dimensional electron gas, large out-of-plane spin polarization is observed in these surfaces which are caused by the anisotropic in-plane charge distribution around the Au atoms [28]. Despite the similarity of the Si(111)5 × 2-Au with these Au-deposited vicinal Si(111) surfaces, no clear evidence of band splitting can be detected by ARPES in the Si(111)5 × 2-Au. On the other hand, a clear splitting of surface state band by the Rashba effect has been recently reported on the other Au-induced reconstructed surfaces on Si(111), the Si(111)$\sqrt{3} \times \sqrt{3}$-Au, with the coadsorption of small amount of different metal in which the formation of domain walls is suppressed and the real nature inside the domain can be observed [31].

In this paper, we have investigated the spin polarization of surface electronic states of Si(111)5 × 2-Au by means of spin-resolved ARPES (spin-ARPES) measurement. By virtue of spin resolution, experimental evidence of spin polarization is clearly observed in all the surface states of the system. The spin-polarization reversal with respect to the $\overline{\Gamma}$ point signifies the Rashba origin of the spin polarization. In addition to the typical in-plane helical spin polarization, significant out-of-plane spin polarization is observed in some of the surface states. These experimental results are compared with the first-principles calculation based on the recently proposed new model of Si(111)5 × 2-Au (=KK model). The fair agreement of the spin texture by the experiment and the calculation supports the KK model as the most plausible model for the surface reconstruction.

II. EXPERIMENT

Single-domain Si(111)5 × 2-Au surface was obtained by evaporating Au on vicinal clean Si(111) surface that is offcut 1.8° along [11$\bar{2}$] direction, in the ultrahigh vacuum (3×10^{-8} Pa) chamber. Cleaning of the vicinal Si(111) surface was done by the special annealing procedure to obtain regular step arrays, which is reported by Viernow *et al.* [32].

Au was evaporated on to the clean Si surface at 730 °C followed by 10 min postannealing at the same temperature. The optimum amount of Au was estimated by LEED observation.

Clear LEED spots with 5 × 1 periodicity and faint streak at ×2 periodicity as well as the residual very weak 7 × 7 spots were observed as shown in Fig. 1(a), which suggests the subtle shortage of Au amount for the completion of the 5 × 2 reconstruction. The small shortage of Au than the completion of 5 × 2 reconstruction ensures the absence of the effect of SOI from the excess Au atoms. No significant contribution of different domains rotating $\pm 2\pi/3$ was detected in the LEED pattern by virtue of using vicinal Si(111) surface. ARPES and spin-ARPES measurements were done at the ESPRESSO end station [33], beamline 9B of Hiroshima Synchrotron Radiation Center (HiSOR) where we can do three-dimensional spin vectorial analysis of electron spin using double VLEED

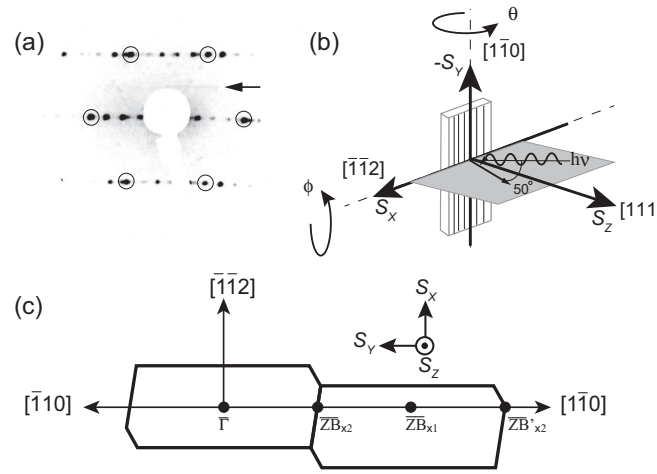

FIG. 1. (a) LEED pattern of Si(111)5 × 2-Au taken at E_k = 45 eV. 1 × 1 fundamental spots are marked with circles. Almost single-domain ×5 spots and weak ×2 streaks (indicated by arrow) are observed in addition with weak ×7 spots. (b) Geometry of (spin-)ARPES measurement. *p*-polarized light impinged into the sample with 50° from the direction of electron analyzer lens. (c) Surface Brillouin zone (SBZ) of Si(111)5 × 2 structure. We named the symmetry points of SBZ crossing with [1$\bar{1}$0] direction as $\overline{ZB}_{\times 2}$, $\overline{ZB}_{\times 1}$, $\overline{ZB}_{\times 2'}$ and so on in accordance with the previous papers [11,23]. The definitions of spin directions in our spin-ARPES measurement and the first-principles calculation (S_X, S_Y, and S_Z) are also indicated with solid and dashed arrows.

(very low-energy electron diffraction) spin detectors with a high-resolution hemispherical analyzer (Scienta R4000) [34]. All the ARPES and spin-ARPES data shown here were taken at the sample temperature of about 100–110 K. In the photoemission measurements, horizontally polarized light of hν = 34 eV, which is the photon energy to enhance the surface states [22] probably due to the photoemission matrix element effect, from the APPLE II type undulator [35] was impinged onto the sample in the experimental geometry shown in Fig. 1(b). Energy and angular resolutions were set as ΔE = 35 meV and $\Delta\theta = \pm 0.3°$ and ΔE = 60 meV and $\Delta\theta = \pm 1.5°$ for ARPES and spin-ARPES measurements, respectively. The effective Sherman functions (S_{eff}) of the spin detectors were 0.3.

III. METHOD OF CALCULATION

DFT electronic structure calculations for the KK model of Si(111) 5 × 2-Au are performed by using all-electron full-potential linearized augmented plane-wave (FLAPW) method [36,37]. Exchange and correlation are treated in the generalized gradient approximation (GGA) with the Perdew-Burke-Ernzerhof form [38]. Dangling bonds of Si in the bulk side of the model are fully terminated by additional H atoms to prevent disturbance in the energy region around surface states. SOI is included in the second-variation step of the self-consistent iterations. Electron density plots with the surface atomic structure are depicted with the three-dimensional (3D) visualization program VESTA [39].

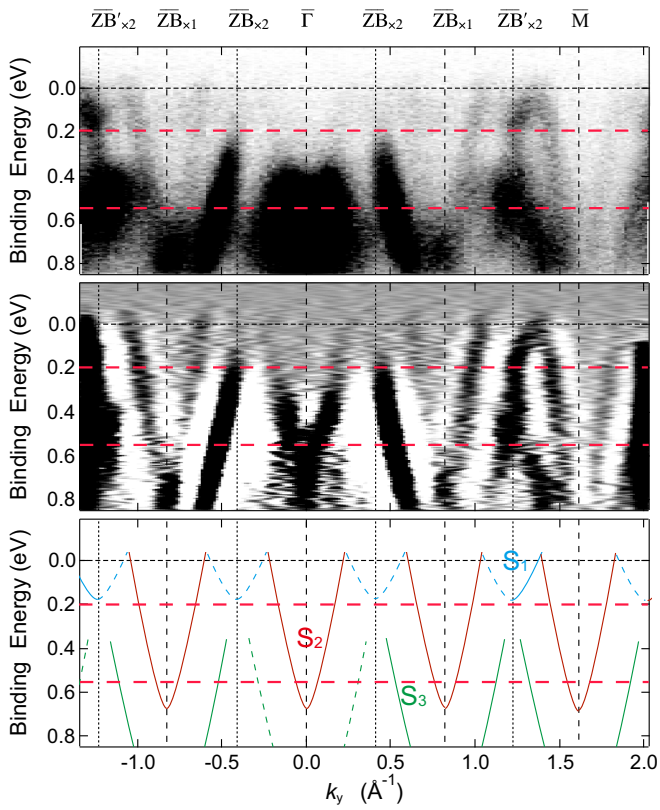

FIG. 2. The band dispersion of Si(111)5 × 2-Au obtained by ARPES measurement taken at hν = 34.0 eV (top panel) at 100 K. Darker means higher photoelectron intensity. The middle panel shows the second derivative of the raw ARPES data to emphasize the observed band structure. The bottom panel indicates the schematic of the observed band structure as a guide to the eyes. Only the bands with solid lines are clearly observed due to the matrix element effect in the photoemission process. The binding energies where the constant energy contours were measured in Fig. 3 are indicated by red lines in the top panel.

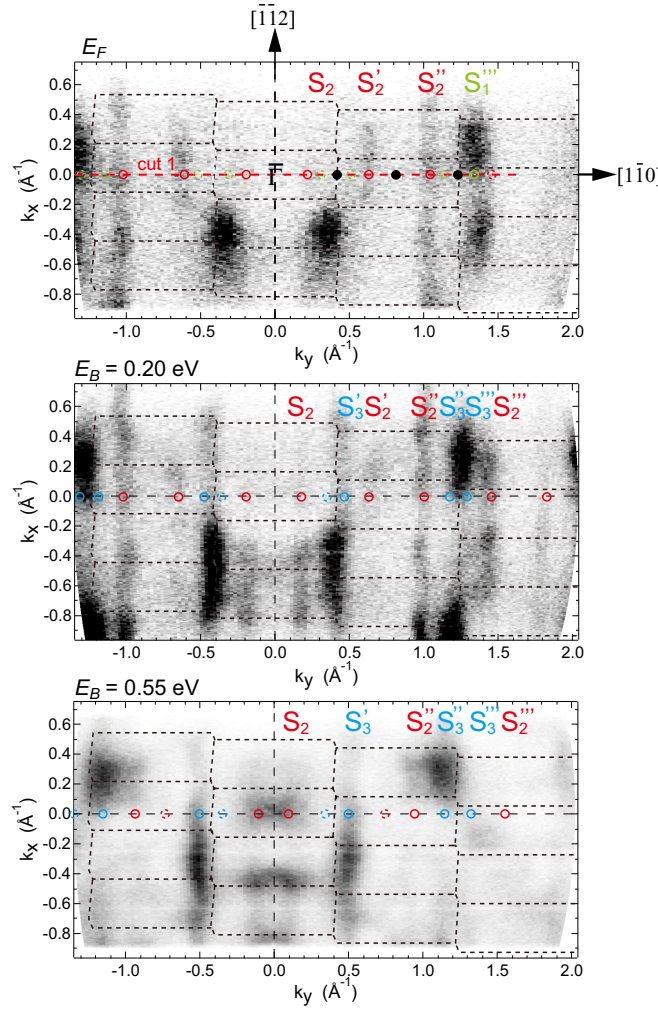

FIG. 3. Constant energy contours of Si(111)5 × 2-Au band at the E_F, E_B = 0.20 eV, and E_B = 0.55 eV taken at hν = 34.0 eV. Darker means higher photoelectron intensity. Surface Brillouin zones of 5 × 2 are overlayed.

IV. RESULTS AND DISCUSSION

Figure 2 shows the band dispersion (energy vs momentum mapping) of the Si(111)5 × 2-Au surface taken along the [1$\bar{1}$0] direction which is parallel to the Au chain. The data have been extracted from a full $E(k_x, k_y)$ map which is taken by rotating the sample with respect to [$\bar{1}\bar{1}$2] axis [i.e., ϕ rotation in Fig. 1(b)]. The top panel is the raw data where the darker part indicates the higher photoelectron intensity. In the middle panel, the image of the second derivative of the raw data is shown to emphasize the feature of the band structure. Several metallic bands are observed which appear repeatedly with the periodicity of 5 × 2 surface Brillouin zones (SBZs). In addition, the other strong bands that disperse almost in parallel to the metallic bands as well as the other faint metallic band at around the zone boundary of SBZ ($\overline{ZB}'_{\times 2}$) are observed. The schematic band structure deduced from the data is indicated in the bottom panel and the bands are categorized into three main surface states (S_1, S_2, S_3) in accordance with the previous paper [20]. The overall features of the observed bands are in good agreement with the previous reports [22,23]. However, in contrast to the asymmetric intensity distribution with respect to the $\overline{\Gamma}$ point reported in the previous studies [22,23], the observed photoemission intensity distribution is symmetric with respect to the $\overline{\Gamma}$ point in our measurement. This difference comes from so-called photoemission matrix element effect with different experimental geometries and we confirmed that the data taken with the same geometry to the previous studies show similar photoemission intensity distributions to the previous paper [see Fig. 1S in Supplemental Material (SM) [40]].

In Fig. 3, the Fermi surface and constant energy contours (CEC) of the bands at the binding energies of E_B = 0.20 and 0.55 eV that are indicated in Fig. 2 with (red) dashed lines are shown. In the figure, the darker region means higher photoemission intensity and SBZs of 5 × 2 unit are also superimposed. Since the data have been taken by the ϕ rotation with respect to [$\bar{1}\bar{1}$2] as mentioned already, the intensity distribution is symmetric with respect to the [$\bar{1}\bar{1}$2] line but asymmetric with respect to the [1$\bar{1}$0] line . As shown in the figure, the one-dimensional character of the bands is

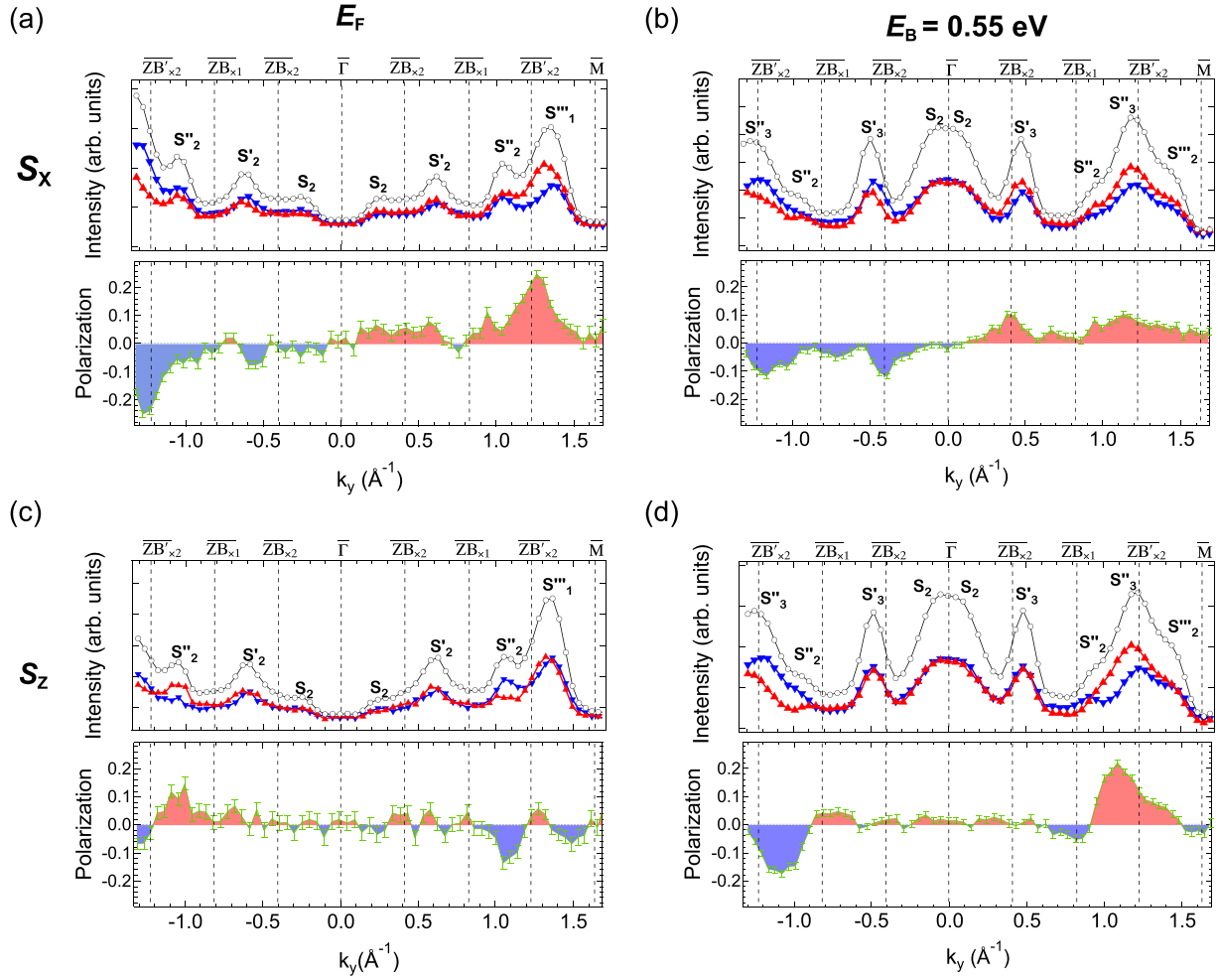

FIG. 4. Spin-resolved momentum distribution curves (spin-MDC) taken at (a), (c) the Fermi level (E_F) and (b), (d) the binding energy (E_B) of 0.55 eV along cut 1 indicated in Fig. 3. Spin-MDC. Both spin components along x and z directions (S_X and S_Z) in the sample coordination have been measured [(a), (b) and (c), (d)]. Red and blue triangles correspond to up- and down-spin MDC spectra. The black curves are the spin-integrated MDC spectra that are the sum of these up and down MDC spectra. Prominent peaks and shoulders are surface states indicated with arrows in Fig. 3. The states in different SBZ are indicated by a prime and double prime, etc. (e.g., S'_2, S''_2, and so on.). The spin polarization determined by $\frac{1}{S_{\text{eff}}}(I_{\text{up}} - I_{\text{down}})/(I_{\text{up}} + I_{\text{down}})$ of each spin-MDC measurement with error bars is also shown at the bottom of each panel.

clearly observed as the straight lines with small undulation in CEC, especially at E_F and $E_B = 0.20$ eV. In contrast, at $E_B = 0.55$ eV some bands especially near $\overline{\Gamma}$ are broadened along k_y being consistent with the previously reported possible transition from one-dimensional to a two-dimensional electronic structure at higher binding energies [11].

In order to examine the spin polarization of the states, we have measured the spin-resolved momentum distribution curves (spin-MDCs) along the one-dimensional chain direction ([$1\bar{1}0$] direction (cut 1 in Fig. 3). Note that although the line is along the one-dimensional chain, it is not along the symmetry line in the SBZ as shown in Fig. 3. Therefore, the observed k points (i.e., lines) are not equivalent in different 5×2 SBZ. Thus, we distinguish the observed prominent surface states at different k_y position as labeled S_2, S'_2, S''_2, etc.

Figure 4 shows the results of the spin-MDC measurement taken at E_F [Figs. 4(a) and 4(c)] and $E_B = 0.55$ eV [Figs. 4(b) and 4(d)]. In the figure, the upper panels [Figs. 4(a) and 4(b)] show the data of the spin component along x axis ($= S_X$) that is parallel to [$\bar{1}\bar{1}2$] direction (see Fig. 1) which corresponds to the in-plane tangential direction of the CEC. While the lower panels [Figs. 4(c) and 4(d)] show the results for the spin component along z axis ($= S_Z$) which is perpendicular to the surface ([111] direction). Since the spin polarization of S_Y component is small compared with the S_X and S_Z, we mainly observed S_X and S_Z spin components in the experiment (see Fig. 2S and SM No. 2 for the detailed information [40]).

In each figure, the intensities of total photoemission (black circle), spin-up state (red up-pointing triangles) and spin-down state (blue down-pointing triangles) as the function of momentum (k_y) are presented. Prominent peaks and shoulders of the total intensity correspond to the surface states as labeled in the figure which is also indicated in Fig. 3 with solid circles. In addition, the momentum dependence of spin polarization is also shown at the lower part of each figure. [The spin

polarization along z axis in the sample coordination (=S_Z) was converted from the data in the detector coordination using the Euler rotation conversion as in Ref. [41] (see SM No. 2 [40]).

Roughly, the momentum dependence of spin polarization is antisymmetric with respect to the $\overline{\Gamma}$ point in all the data set and not periodic with the SBZs. The characteristic momentum dependence probably results from the combination of the symmetric intensity distribution of MDC with respect to the $\overline{\Gamma}$ point which is caused by the photoemission matrix element effect and the peak shift in k space caused by the Rashba effect as explained in detail in the Supplemental Material (see Fig. 3S in the SM No. 3 [40]).

In more detail, in the case of in-plane tangential spin component (=conventional Rashba spin component for the ideal two-dimensional electron gas), clear spin polarization is observed both at E_F and $E_B = 0.55$ eV as in Figs. 4(a) and 4(b). Comparing the peak positions of spin-up and -down states, small but obvious peak shifts are observed especially at S_2' and S_1''' states at E_F and S_3' and S_3'' states at $E_B = 0.55$ eV. At the peaks of S_2', even the sign reversal of spin polarization from negative (positive) to positive (negative) across the peak at $k_y \sim -0.7$ Å^{-1} ($k_y \sim 0.7$ Å^{-1}) is observed at E_F in the S_X component [see Fig. 4(a)]. On the other hand, the shifts of S_2 and S_2'' states are not clear both at E_F and $E_B = 0.55$ eV [Figs. 4(a) and 4(b)]. Although the peak shifts are small, the results of spin-polarization reversal with respect to $\overline{\Gamma}$ point and the same direction of the peak shifts both at E_F and $E_B = 0.55$ eV strongly suggest that the origin of the spin polarization is Rashba effect.

In addition to the in-plane spin polarization, some out-of-plane spin polarization (S_Z) is obviously observed as shown in Figs. 4(c) and 4(d). Significant spin polarizations and some peak shifts are observed, especially in the S_2'' state both at E_F and $E_B = 0.55$ eV, and in the S_3'' state at $E_B = 0.55$ eV. However, only small polarization is observed in the states near the $\overline{\Gamma}$ point (i.e., S_2 and S_3'). The overall spin polarization is again reversed with respect to $\overline{\Gamma}$ point being consistent with the spin polarization induced by Rashba effect. The existence of the out-of-plane spin components is in agreement with the similar Au chain system such as Si(553)-Au [29] or Si(557)-Au [28] and probably caused by the in-plane asymmetric charge distribution around the Au atoms as will be discussed later in detail.

As mentioned already, in contrast with the S_X and S_Z components, only small spin polarization is observed in the radial component (S_Y) being consistent with the Rashba picture.

In order to further reveal the characteristic of spin-polarized surface states, we estimated the magnitude and angle of spin polarization as the function of momentum both at E_F and $E_B = 0.55$ eV in Fig. 5. In the figure, we plotted $S_{tot} = \sqrt{S_X^2 + S_Z^2}$ as the magnitude of spin polarization since the contribution of S_Y is relatively small compared with S_X and S_Z. The orientation of the spin vector is also plotted in Fig. 5(c) (at E_F) and 5(d) (at $E_B = 0.55$ eV) where the magnitude of the spin polarization is also indicated by the size of the circles in each plot. In the figure, the color of circles is coded with the color of total MDC. With these plots we can more easily understand that the surface states in the different SBZ possess different magnitude and/or spin orientation. For

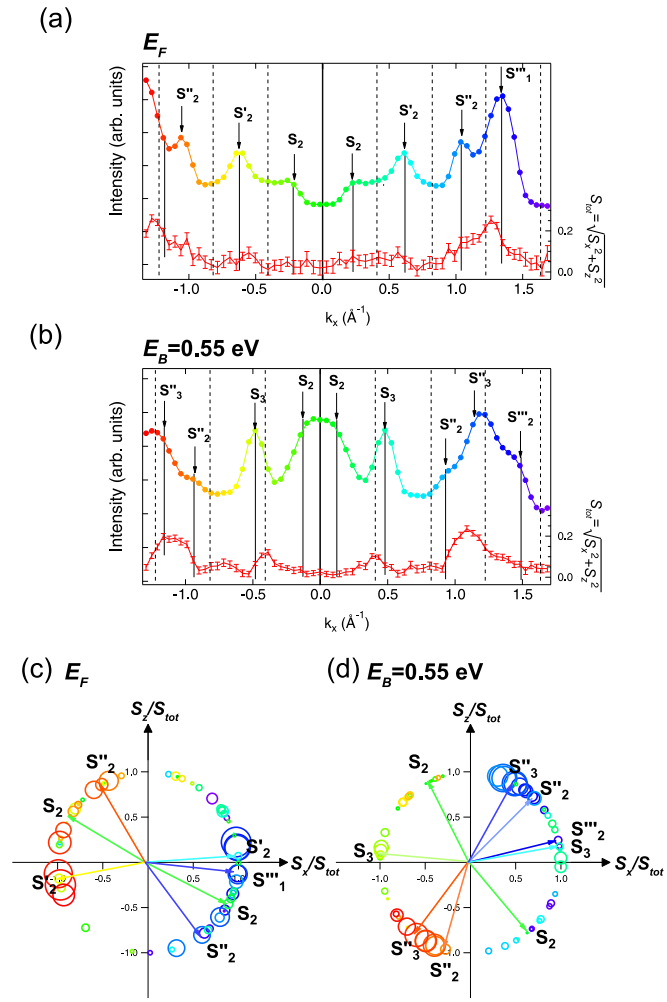

FIG. 5. Absolute value of spin-polarization vector ($S_{tot} = \sqrt{S_X^2 + S_Z^2}$) as the function of momentum that is obtained from the x- and z-spin components S_X and S_Z in Fig. 4 at (a) E_F and (b) $E_B = 0.55$ eV. Direction of spin vector (S_X/S_{tot}, S_Z/S_{tot}) as the function of momentum are also plotted in (c) E_F and (d) $E_B = 0.55$ eV. The color of circles is coded with the color of MDC curves in (a) and (b). The magnitude of the spin-polarization vector (=S_{tot}) at each point is also indicated with the size of each circle.

example, as in Figs. 5(a) and 5(c), at E_F, though all the S_2 states in different SBZ show the low magnitude of spin polarization, the spin orientation changes dramatically from in-plane (S_2') to almost perpendicular (S_2'') and S_2 is pointing in-between both the S_2' and S_2'' states. At $E_B = 0.55$ eV, the magnitude of spin polarization of S_2 state is again not high but the spin orientation shows some variations. That is, S_2 and S_2'' show significant out-of-plane spin polarization but S_2''' shows almost in-plane spin polarization. Compared with the S_2 states, S_3 and S_1 states show relatively high magnitude of spin polarization and the spin orientation is almost in plane in the S_3 and S_1''' states, but S_3''' state shows quite high out-of-plane spin polarization. Note that although the spin orientation is depending very much on the momentum even in the same surface states, almost π difference of spin orientation angles of each pair of surface states having opposite k values is consistent with the Rashba-type spin polarization.

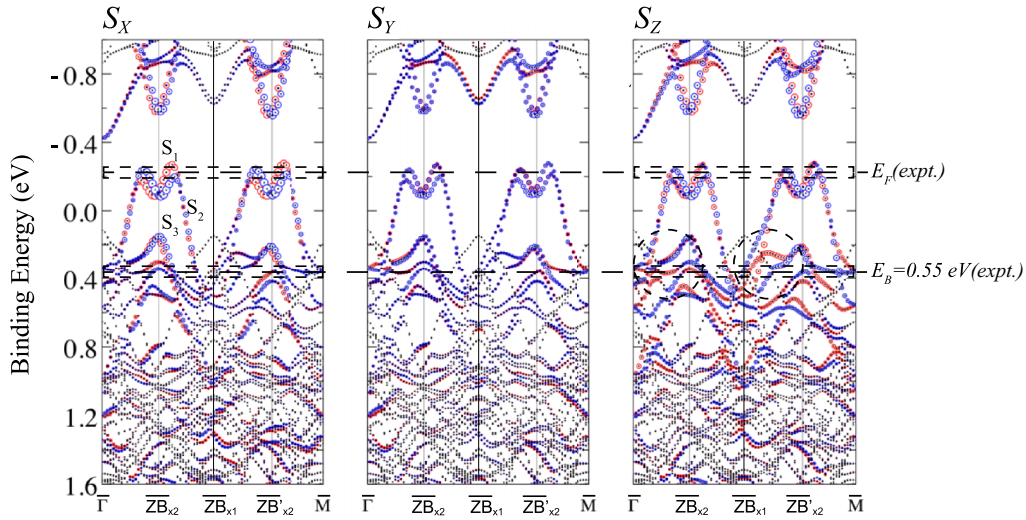

FIG. 6. Spin-resolved band structures of the Si(111)5 × 2-Au based on the KK model by the first-principles calculation including SOI. Red and blue circles mean up- and down-spin components, respectively. The size of the circles indicates the degree of spin polarization. The axes of spin polarization in the calculation correspond to the S_X, S_Y, and S_Z directions indicated in Fig. 1(c). The calculated Fermi energy is set to the origin of the vertical axis.

To understand the observed characteristic spin polarization depending on the surface states and **k** positions, we have calculated the spin-resolved band structure by the first-principles calculation. Figure 6 shows the calculated band dispersion based on the KK model [20] with including SOI. Comparing with the computed results, the experimentally observed Fermi level is about 220 meV higher than the calculated one as indicated with the dashed line in Fig. 6 [E_F(expt.)]. As discussed in Ref. [20], the shift of the Fermi level can be explained by considering the electron donation from Si adatoms.

Except for the Fermi energy difference, the calculated results reproduced well the observed dispersion of the surface states (S_1, S_2, and S_3) and are also in good agreement with the previous calculation by Kwon and Kang [20]. However, different from the previous calculation which is without including SOI, some band splitting appears in the present calculation due to the SOI. The red and blue circles in the figure correspond to the spin-up and -down states, and the size of the circles indicates the degree of spin polarization (larger is higher spin polarization). One can see a clear difference in the degree of spin polarization between S_x, S_y, and S_z spin components in the calculation. The largest (smallest) spin polarization is obtained in S_x (S_y) component being consistent with the experimental results and Rashba picture.

The calculation shows that the shifts between spin-up and -down states are relatively larger in S_1 and S_3 compared with those of S_2. Relatively larger magnitude of spin polarization in S_1'' at E_F and S_3 and S_3'' at $E_B = 0.55$ eV than the S_2 state observed in the experiment (Fig. 5) are in good agreement with the calculation.

The calculated results also show the significant out-of-plane spin polarization (S_Z) which is in agreement with the experimental results. At the E_F(expt.), existence of out-of-plane spin polarization is reproduced both in S_1 and S_2 states. In case of S_2, even higher spin polarization in S_Z than that in S_X is expected by the calculation and the large spin polarization in S_Z than in S_X observed in S_2'' states are compatible with the calculation.

Furthermore, the observed transition from in-plane spin orientation (S_3) to out-of-plane spin orientation (S_3'') in the S_3 state at $E_B = 0.55$ eV is well reproduced by the calculation. Namely, in the calculation, at higher binding energies, S_X is dominant in the S_3 state near the $\bar{\Gamma}$ point, but S_Z becomes stronger in the second SBZ being in good agreement with the experimental results.

In addition, in the calculation, at the higher binding energies, the band structure is more asymmetric than the one near E_F. That is, the band dispersion in the k region from $\overline{ZB}_{\times 1}$ to $\overline{ZB'}_{\times 2}$ at the binding energies higher than 0.2 eV(calc.) is deformed from the band dispersions near the $\bar{\Gamma}$ point both in S_2 and S_3 states (see around the dashed circles indicated in Fig. 6). These band structure deformations are accompanying the large band split between different spin states, especially in the region from $\overline{ZB}_{\times 1}$to $\overline{ZB'}_{\times 2}$. The observed out-of-plane spin polarization of S_2'' and strong spin polarization in S_3''' at $E_B = 0.55$ eV which are in the area between $\overline{ZB}_{\times 1} - \bar{M}$ are consistent with the large spin polarization in S_Z component caused by the band dispersion deformation in the calculation. Furthermore, the sign change of S_2'' state in S_Z component between E_F and $E_B = 0.55$ eV [see Figs. 5(c) and 5(d)] is also reproduced as the opposite band shifts between spin-up and -down states at E_F(expt.) and $E_B = 0.55$ eV(expt.) by the calculation. The overall agreement of the spin polarization and the band structure between the experimental observation and the calculation strongly supports the KK model as the plausible structural model for the Si(111)5 × 2-Au surface.

As shown in the above discussion, the calculation shows clearly that the band dispersion is modified in the different SBZ which accompanies the change of spin polarization in magnitude and orientation among different SBZs being consistent with the experimental observation. Since the band deformation among different SBZs is stronger at higher

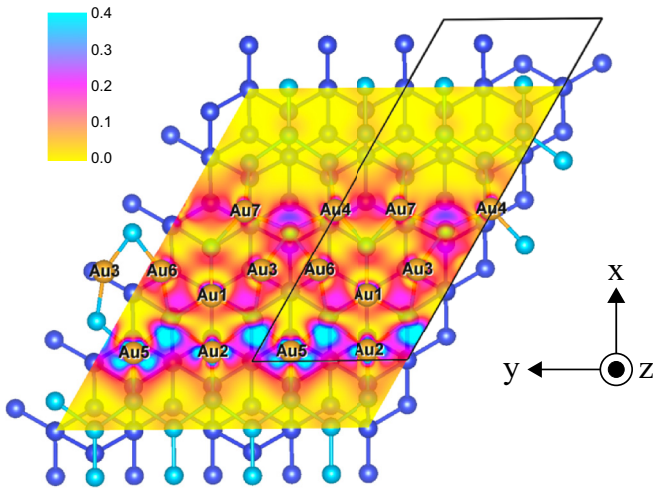

FIG. 7. Electron density of the wave functions around the Fermi energy calculated based on the KK model. The electron density is drawn on the *x*-*y* plane with the averaged height (z) of all Au adatoms. Color codes from yellow to cyan are scaled from 0.0 to $0.4e/\text{bohrs}^3$.

binding energies where the surface states change into surface resonant states, the spin-polarization variation among different SBZs probably comes from the interaction between the surface states and the substrate states, which might be related to the transition from one-dimensional to two-dimensional electronic structure observed in the previous study [11]

Finally, we would discuss briefly the origin of out-of-plane spin polarization. In Fig. 7 we present the charge distribution at E_F(calc.) obtained from the first-principles calculation. In the figure, magenta (yellow) means the part where the charge density is highest (lowest). The obtained results are in good agreement with the charge distribution of S_1 and S_2 states of the previous calculation by Kwon and Kang [20]. According to the calculation, the metallic one-dimensional bands (S_1 and S_2) are mainly caused by the hybridization of Au2 and Au5 atoms with substrate Si atoms. Thus, the surface states can be modified strongly at higher binding energies as discussed above (see also SM No. 5 [40]). On the contrary, the hybridization of Au1 and Au3 atoms with Si substrate is weaker than the case of Au2 and Au5. Further, in the case of Au4 and Au7, the hybridization with neighboring Au is dominant and causes bonding and antibonding states. Thus, these Au atoms do not contribute to the metallic S_1 and S_2 bands. Focusing on the states dominated by Au2 and Au5, the in-plane charge distribution is not homogeneous but quite asymmetric around the Au atoms. Thus, similar to the case of Si(557)-Au surface [28], the anisotropic in-plane charge distribution can be the cause of observed large out-of-plane spin polarization.

V. CONCLUSION

In conclusion, we have examined spin polarization of the surface states of Si(111)5 × 2-Au by means of spin- and angle-resolved photoelectron spectroscopy and the first-principles calculation including spin-orbit interaction. By spin-ARPES measurement, small but clear spin polarization has been observed in in-plane tangential (conventional Rashba) spin component which is perpendicular to the Au chain structure. Antisymmetric spin polarization with respect to the $\overline{\Gamma}$ point and the k shift of spin-up and -down components at each surface state suggest the Rashba-effect origin of the spin polarization which is caused by the strong spin-orbit interaction of Au. In addition, significant spin polarization is observed also in the out-of-plane spin components, which is probably caused by the asymmetric in-plane charge distribution around Au atoms. The degree of spin polarization and spin orientation in some surface states depend on the **k** position in SBZ probably due to the interaction with Si substrate. The observed spin polarization is qualitatively well reproduced both in in-plane and out-of-plane components by the first-principles calculation including spin-orbit interaction based on the recently proposed structural model by Kwon and Kang suggesting its validity. The finding of a new quasi-one-dimensional metallic spin-polarized band on semiconductor expands the variety of materials for the spintronic devices. Since the metallic surface states are on the semiconductor substrate, the system might be much more suitable to investigate the spin-polarized one-dimensional transport than the system on the metallic substrate such as previously reported quasi-one-dimensional state on Bi(114) [42] and can provide the new playground for the investigation of the spin-polarized electron in one-dimensional systems.

ACKNOWLEDGMENTS

The authors appreciate very much Prof. M. Ho Kang and Dr. S. Gab Kwon for their kind provision of atomic structural data of the KK model for the first-principles calculation and the fruitful discussion. This work was partly supported by KAKENHI (Grants No. 19340078, No. 16H02114, No. 17H06254, and No. 23244066), Grant-in-Aid for Scientific Research (B), (A) and (S) of Japan Society for the Promotion of Science. The experiments were performed with the approval of the Proposal Assessing Committee of the Hiroshima Synchrotron Radiation Center (Proposal No. 15-B-10).

[1] H. S. Yoon, S. J. Park, J. E. Lee, C. N. Whang, and I.-W. Lyo, Phys. Rev. Lett. **92**, 096801 (2004).
[2] P.-G. Kang, H. Jeong, and H. W. Yeom, Phys. Rev. Lett. **100**, 146103 (2008).
[3] I. Barke, S. Polei, V. V. Oeynhausen, and K.-H. Meiwes- Broer, Phys. Rev. Lett. **109**, 066801 (2012).
[4] H. Lipson and K. E. Singer, J. Phys. C: Solid State Phys. **7**, 12 (1974).
[5] L. D. Marks and R. Plass, Phys. Rev. Lett. **75**, 2172 (1995).
[6] T. Hasegawa, S. Hosaka, and S. Hosoki, Surf. Sci. **357**, 858 (1996).
[7] S. C. Erwin, Phys. Rev. Lett. **91**, 206101 (2003).

[8] H. Daimon, C.-I. Chung, S. Ino, and Y. Watanabe, Surf. Sci. **235**, 142 (1990).

[9] A. A. Baski, J. Nogami, and C. F. Quate, Phys. Rev. B **41**, 10247(R) (1990).

[10] J. D. O'Mahony, C. H. Patterson, J. F. McGilp, F. M. Leibsle, P. Weightman, and C. F. J. Flipse, Surf. Sci. Lett. **277**, L57 (1992).

[11] R. Losio, K. N. Altmann, and F. J. Himpsel, Phys. Rev. Lett. **85**, 808 (2000).

[12] M. Kang and J. Y. Lee, Surf. Sci. **531**, 1 (2003).

[13] S. Riikonen and D. Sanchez-Portal, Phys. Rev. B **71**, 235423 (2005).

[14] C.-Y. Ren, S.-F. Tsay, and F.-C. Chuang, Phys. Rev. B **76**, 075414 (2007).

[15] F.-C. Chuang, C.-H. Hsu, C.-Z. Wang, and K.-M. Ho, Phys. Rev. B **77**, 153409 (2008).

[16] I. Barke, F. Zheng, S. Bockenhauer, K. Sell, V. V. Oeynhausen, K. H. Meiwes-Broer, S. C. Erwin, and F. J. Himpsel, Phys. Rev. B **79**, 155301 (2009).

[17] S. C. Erwin, I. Barke, and F. J. Himpsel, Phys. Rev. B **80**, 155409 (2009).

[18] T. Abukawa and Y. Nishigaya, Phys. Rev. Lett. **110**, 036102 (2013).

[19] C. Hogan, E. Ferraro, N. McAlinden, and J. F. McGilp, Phys. Rev. Lett. **111**, 087401 (2013).

[20] S. G. Kwon and M. H. Kang, Phys. Rev. Lett. **113**, 086101 (2014).

[21] T. Shirasawa, W. Voegeli, T. Nojima, Y. Iwasawa, Y. Yamaguchi, and T. Takahashi, Phys. Rev. Lett. **113**, 165501 (2014).

[22] K. N. Altmann, J. N. Crain, A. Kirakosian, J. L. Lin, D. Y. Petrovykh, F. J. Himpsel, and R. Losio, Phys. Rev. B **64**, 035406 (2001).

[23] I. Matsuda, M. Hengsberger, F. Baumberger, T. Greber, H. W. Yeom, and J. Osterwalder, Phys. Rev. B **68**, 195319 (2003).

[24] J. L. McChesney, J. N. Crain, V. Pérez-Dieste, F. Zheng, M. C. Gallagher, M. Bissen, C. Gundelach, and F. J. Himpsel, Phys. Rev. B **70**, 195430 (2004).

[25] J. N. Crain, A. Kirakosian, K. N. Altmann, C. Bromberger, S. C. Erwin, J. L. McChesney, J.-L. Lin, and F. J. Himpsel, Phys. Rev. Lett. **90**, 176805 (2003).

[26] J. N. Crain, J. L. McChesney, F. Zheng, M. C. Gallagher, P. C. Snijders, M. Bissen, C. Gundelach, S. C. Erwin, and F. J. Himpsel, Phys. Rev. B **69**, 125401 (2004).

[27] I. Barke, F. Zheng, T. K. Rugheimer, and F. J. Himpsel, Phys. Rev. Lett. **97**, 226405 (2006).

[28] T. Okuda, K. Miyamoto, Y. Takeichi, H. Miyahara, M. Ogawa, A. Harasawa, A. Kimura, I. Matsuda, A. Kakizaki, T. Shishidou, and T. Oguchi, Phys. Rev. B **82**, 161410(R) (2010).

[29] H. W. Yeom, S. W. Jung, J. S. Shin, J. Kim, K. S. Kim, K. Miyamoto, T. Okuda, H. Namatame, A. Kimura, and M. Taniguchi, New J. Phys. **16**, 093030 (2014).

[30] D. Sanchez-Portal, S. Riikonen, and R. M. Martin, Phys. Rev. Lett. **93**, 146803 (2004).

[31] L. V. Bondarenko, D. V. Gruznev, A. A. Yakovlev, A. Y. Tupchaya, D. Usachov, O. Vilkov, A. Fedorov, D. V. Vyalikh, S. V. Eremeev, E. V. Chulkov, A. V. Zotov, and A. A. Saranin, Sci. Rep. **3**, 1826 (2013).

[32] J. Viernow, J.-L. Lin, D. Y. Petrovykh, F. M. Leibsle, F. K. Men, and F. J. Himpsel, Appl. Phys. Lett. **72**, 948 (1998).

[33] T. Okuda, K. Miyamaoto, H. Miyahara, K. Kuroda, A. Kimura, H. Namatame, and M. Taniguchi, Rev. Sci. Instrum. **82**, 103302 (2011).

[34] T. Okuda, K. Miyamoto, A. Kimura, H. Namatame, and M. Taniguchi, J. Electron Spectros. Relat. Phenomena **201**, 23 (2015).

[35] S. Sasaki, A. Miyamoto, K. Goto, M. Arita, T. Okuda, T. Mitsuyasu, K. Fujioka, H. Namatame, and M. Taniguchi, J. Phys.: Conf. Ser. **425**, 032009 (2013).

[36] E. Wimmer, H. Krakauer, M. Weinert, and A. J. Freeman, Phys. Rev. B **24**, 864 (1981).

[37] J. M. Soler and A. R. Williams, Phys. Rev. B **40**, 1560 (1989).

[38] J. P. Perdew, K. Burke, and M. Ernzerhof, Phys. Rev. Lett. **77**, 3865 (1996).

[39] K. Momma and F. Izumi, J. Appl. Crystallogr. **44**, 1272 (2011).

[40] See Supplemental Material at http://link.aps.org/supplemental/10.1103/PhysRevB.101.045430 for the band dispersion taken with the same experimental geometry to the previous papers, the comparison of *x,y*, and *z* spin component in spin-MDC measurement, the way of conversion from detector coordination to the sample coordination, the simulation of antisymmetric spin-polarization with respect to the $\bar{\Gamma}$ point, the contribution of each Au atom to the surface state bands, and the calculated electron density of the wave functions at different binding energies.

[41] M. Hoesch, T. Greber, V. N. Petrov, M. Muntwiler, M. Hengsberger, W. Auwärter, and J. Osterwalder, J. Electron Spectros. Relat. Phenomena **124**, 263 (2002).

[42] J. W. Wells, J. H. Dil, F. Meier, J. Lobo-Checa, V. N. Petrov, J. Osterwalder, M. M. Ugeda, I. Fernandez-Torrente, J. I. Pascual, E. D. L. Rienks, M. F. Jensen, and Ph. Hofmann, Phys. Rev. Lett. **102**, 096802 (2009).